

## Solution-chemistry control of Mg<sup>2+</sup>-calcite interaction mechanisms: Implication for biomineralization

JIE XU<sup>1,\*</sup>, JIANHUA WANG<sup>2</sup>, MINA HONG<sup>3</sup>, AND H. HENRY TENG<sup>3,\*</sup>

<sup>1</sup>Geosciences Department, Virginia Tech, Blacksburg, Virginia 24060, U.S.A.

<sup>2</sup>Department of Terrestrial Magnetism, Carnegie Institutions of Washington, Washington, D.C. 20015, U.S.A.

<sup>3</sup>Chemistry Department, George Washington University, Washington, D.C. 20052, U.S.A.

### ABSTRACT

We investigated the effect of Mg<sup>2+</sup> on calcite hillock growth over a broad range of solution conditions in terms of supersaturation ( $\Omega_{\text{calcite}}$ ) and Mg/Ca ratios using atomic force microscopy and secondary ion mass spectrometry. We found that both the incorporation pattern/incorporated Mg<sup>2+</sup> quantity in the hillock structure and the Mg<sup>2+</sup>-induced morphological change of the hillock surface showed strong dependence of the growth conditions. Specifically, when Mg/Ca was high (i.e., >5) and  $\Omega_{\text{calcite}}$  was low (i.e., ~0.45), Mg<sup>2+</sup> was predominantly incorporated into the negative sectors of the hillock structure, resulting in gradual loss of step structure and morphological amorphism on these vicinal surfaces. When Mg/Ca and  $\Omega_{\text{calcite}}$  were in intermediate ranges (i.e., Mg/Ca < 5, and 0.45 <  $\Omega_{\text{calcite}}$  < 1), the originally straight edges of the hillock steps exhibited curvatures of varying degrees and formed “tear-drop” morphologies. It is noted that such “tear-drop” morphology was stable within the duration of the experiments and did not evolve into other surface patterns. By contrast, when both Mg/Ca and  $\Omega_{\text{calcite}}$  were high (i.e., Mg/Ca > 5, and  $\Omega_{\text{calcite}}$  > 1.1), the growing hillocks experienced two phases of morphological changes, initiated with the formation of “tear-drops” followed by the development of linear ruptures along  $[\bar{4}81]$  and  $[44\bar{1}]$  directions. And the occurrence of these ruptures segmented the hillock surface effectively into multiple isolated plateaus. Significantly, we revealed the underlying mechanisms for these condition-specific effects of Mg<sup>2+</sup> on calcite growth, which mainly resulted from the interplay among three major factors: (1) the size-mismatch between Mg<sup>2+</sup> and Ca<sup>2+</sup> that causes structural strains in magnesian calcite and leads to morphological amorphism in high-Mg carbonate; (2) the asymmetry of the calcite crystal structure that sets a physical limitation for Mg<sup>2+</sup> incorporation patterns in the hillock structure; and (3) the step advancing rate (i.e., the calcite growth kinetics) that affects both Mg<sup>2+</sup> incorporation and the accommodation of Mg<sup>2+</sup>-induced structural strains in the hillock structure. Detailed discussions were given for each growth scenario. The results of our study provide a theoretical base to decipher the roles of Mg<sup>2+</sup> in CaCO<sub>3</sub> mineralization, and thus, have important implication for a range of processes that involve the growth of Mg-Ca-CO<sub>3</sub> systems, such as biomineralization, carbon capture and storage, and scale controls in industrial settings.

**Keywords:** Mg-Ca-CO<sub>3</sub>, biomineralization, lattice strain and stress

### INTRODUCTION

Mineralization of calcium carbonate (CaCO<sub>3</sub>), a ubiquitous process in natural and anthropogenic settings, can be affected by various trace elements and xeno compounds including metal cations, anions, organic polymers, and biomolecules (Reddy and Nancollas 1976; Mucci and Morse 1983; Reeder 1996; Hemming et al. 1998; Parsiegla and Katz 1999; Astilleros et al. 2000; Davis et al. 2000; Freund et al. 2001; Wasylenki et al. 2005; Lakshatnov et al. 2011; Montes-Hernandez et al. 2011; Xu et al. 2013; Long et al. 2014). Chief among the modifiers in sedimentary environments and calcifying organisms are magnesium cations (Mg<sup>2+</sup>), which were demonstrated to impact the morphology, composition, and crystal structure of the formed CaCO<sub>3</sub> phases. The current scientific interests in the Mg-Ca-CO<sub>3</sub> system mainly stemmed from the close tie of Mg<sup>2+</sup> and CaCO<sub>3</sub> in nature, manifested by the prevalence of Mg-bearing carbonates (i.e., magnesian calcite and dolomite) in geological records, but

also have extended far beyond the traditional sedimentology and mineralogy, well into the biomineralization, paleoclimatology, and material science as well as industrial practices.

It has been well recognized that the presence of Mg<sup>2+</sup> alters the growth morphology of CaCO<sub>3</sub> (i.e., calcite). The best-known correlation between solution Mg<sup>2+</sup> content and calcite growth morphology was reported in early 1970s, when Folk (1974) observed that with increasing Mg/Ca ratios in the growth medium, the resultant calcite crystals were elongated parallel to the *c*-axis. Various models were subsequently proposed to explain this elongation phenomenon (including Folk 1974; Lahann 1978; Given and Wilkinson 1985), and significant attention was directed to the potential selective effect of Mg<sup>2+</sup> on different crystal faces of calcite. The validity of these models remained controversial however, until direct field and experimental evidence became available in late 1980s. One important piece of such evidence was the (intra)sectoral zoning of trace elements (including Mg, Sr, Mn, and etc.) in calcite crystals, identified by Reeder et al. using a range of analytical tools (Reeder and Grams 1987;

\* E-mail: jie7@vt.edu; hteng@gwu.edu

Raven and Dickson 1989; Paquette and Reeder 1990a, 1990b). And follow-up investigations revealed that such (intra)sectoral zoning was caused by a particular (spiral) growth mechanism of calcite, which also forms asymmetric hillocks comprised of nonequivalent ( $\pm$ ) vicinal faces (Paquette and Reeder 1995; Hemming et al. 1998). Teng et al. (1998) confirmed this specific growth mechanism of calcite using in situ atomic force microscopy, and further illustrated the resultant surface structure and crystal habits. It was perhaps Davis et al. (2004) that first provided molecular-level explanation for the elongating effect of Mg<sup>2+</sup> on calcite. Davis et al. (2004) proposed that the differential incorporation of Mg into nonequivalent steps resulted in accumulation of strains at the step intersection, thereby producing new step directions and elongating the calcite crystals. Although being much less referenced in carbonate studies, Mg<sup>2+</sup> was also reported to cause surface segmentation of calcite. Sethmann et al. (2010) found that fast layer-by-layer growth of magnesian calcite on pure calcite induces the formation of networks of ridges along the  $[\bar{4}41]$ ,  $[48\bar{1}]$ , and  $[42\bar{1}]$  directions, and indicated that the segmentation is a way to relax the accumulated strain arising from size mismatch of Mg<sup>2+</sup> and Ca<sup>2+</sup> (a.k.a., Stranski-Krastanov growth mode). Taking a computational approach, Elstnerova et al. (2010) backed the “strain theory” for both phenomena (i.e., elongation and segmentation effects of Mg<sup>2+</sup> on calcite), and demonstrated that random Mg-substitution for Ca in calcite structure increases the structural stiffness and distortion dramatically and prevents crystal formation when Mg content reaches ~45%. A recent experimental work (Xu et al. 2013) on Mg-Ca-CO<sub>3</sub> crystallization in non-aqueous medium showed that the precipitates lose crystallinity when Mg content exceeds ~40%, leading the authors to propose that an intrinsic barrier resulting from a reduced volume in the interstitial space between the smaller Mg octahedra limits Mg<sup>2+</sup> and CO<sub>3</sub><sup>2-</sup> to form long-range orders at ambient conditions.

On a different note, the presence of Mg<sup>2+</sup> is related to the transformations between CaCO<sub>3</sub> polymorphs, i.e., calcite  $\leftrightarrow$  ACC, and calcite  $\leftrightarrow$  aragonite. Multiple groups (e.g., Loste et al. 2003; Nishino et al. 2009; Liu et al. 2013) reported that CaCO<sub>3</sub> precipitates from a supersaturated solution were changed from rhombohedral calcite at low Mg<sup>2+</sup> concentration to spherical ACC at high Mg<sup>2+</sup> concentration. In Nishino et al. (2009), nanocrystalline domains were identified within the ACC spheres, suggesting that the existence of Mg<sup>2+</sup> suppressed the regular crystal growth of calcite nuclei and thus, stabilized the metastable amorphous phase. Depending on the specific experimental conditions, calcite can also be transformed into aragonite in the presence of Mg<sup>2+</sup> (Fernandez-Diaz et al. 1996; Xie et al. 2009; Huang et al. 2012). And the proposed mechanisms also emphasized the inhibitory effect of Mg<sup>2+</sup> on the calcite growth.

Yet, across the different aspects of Mg-Ca-CO<sub>3</sub> research, a comprehensive understanding of the molecular-level interactions between Mg<sup>2+</sup> and CaCO<sub>3</sub> (i.e., calcite) remains elusive, and further, the possible roles of the Mg<sup>2+</sup>-induced strains in transforming the CaCO<sub>3</sub> morphology and crystal structure were not fully appreciated in most of the previous studies. Even in the cases where such strains were suggested to be the controlling factor, how the strains are manifested at advancing steps and affect the growth kinetics under varying solution conditions is

poorly understood. For example, it is not clear why Mg<sup>2+</sup> causes calcite surface segmentation in certain scenarios (e.g., Sethmann et al. 2010) while merely elongates the calcite crystals in some others (e.g., Davis et al. 2004). Thus, these outstanding questions provided major motivation for our current study.

In this study, we examined the effects of Mg<sup>2+</sup> on calcite hillock growth over a broad range of solution conditions (in terms of supersaturation and Mg/Ca ratios) using atomic force microscopy (AFM) and secondary ion mass spectrometry (SIMS). We found that, depending on the calcite growth rates and Mg/Ca ratios in the solution, the presence of Mg<sup>2+</sup> could modify the step morphology and the overall hillock structure in distinct modes. Significantly, we also revealed the specific mechanisms involved in the Mg<sup>2+</sup>-calcite interactions for each scenario. The findings of our study may provide new insight into the crystal growth of Mg-Ca-CO<sub>3</sub> systems and, meanwhile, have implications for a multitude of geochemical, biological, and industrial processes, such as biomineralization, carbon capture and storage, and control of scale formation.

## MATERIALS AND METHODS

### Sample and growth solution preparation

ACS-grade reagents of CaCl<sub>2</sub>·2H<sub>2</sub>O, MgCl<sub>2</sub>, and NaHCO<sub>3</sub> (purchased from Sigma-Aldrich), and ultrapure water (18 M $\Omega$ -cm, Millipore) were used to prepare experimental solutions with various Mg/Ca ratios and supersaturation with respect to calcite (i.e.,  $\Omega_{\text{calcite}}$ ) based on PHREEQC calculations. The supersaturation ( $\Omega$ ) was defined as the logarithm of the ratio of ion activity product (IAP) to solubility product ( $K_{\text{sp}}$ ), and the constant used for the  $K_{\text{sp}}$  of calcite was 10<sup>-8.48</sup>. The details for the solution pH, composition, and supersaturation were listed in Table 1. The ionic strength in the solutions was leveled up to ~0.1 by addition of sodium chloride, and the pH was maintained at 7.8  $\pm$  0.2.

### In-situ AFM experiments

We examined the effect of solution Mg<sup>2+</sup> on calcite growth using an atomic force microscope (AFM) coupled with commercially available silicon nitride (Si<sub>3</sub>N<sub>4</sub>) cantilevers and a flow-through fluid cell. The details for the method has been described elsewhere (Teng et al. 2000). Specifically, the calcite samples for the AFM work (Wards Scientific, Rochester, New York) were cleaved along the {10 $\bar{1}$ 4} surface immediately prior to use. The injected solution with varied Mg/Ca ratios and  $\Omega_{\text{calcite}}$  combinations was also freshly prepared. A consistent flow rate of 30 mL/h via a syringe pump was adopted to minimize the effect of mass transport on calcite growth or on the Mg<sup>2+</sup>-calcite interactions. We started each experiment with injecting a supersaturated solution (i.e.,  $\Omega_{\text{calcite}} = 1.15$ ) free of Mg<sup>2+</sup> to spike the formation of calcite spiral hillocks (Fig. 1). Such hillock structure of calcite provides a good model to study the molecular-level interactions of trace elements and the major crystal faces (of calcite). Once the hillocks reached micrometer sizes (i.e., > 10  $\mu$ m), we changed the Mg-free injection with Mg<sup>2+</sup>-bearing solutions and recorded the corresponding modifications of hillock morphologies.

To measure the advancing rates of the hillock steps, we adjusted the scanning angle and direction accordingly in each experiment (Teng et al. 2000) so that the movement of individual points at one step edge was recorded through a certain period. We used the slope ( $\alpha$ ) of the recorded image to estimate the step velocity, and defined three growth scenarios: (1) when  $\alpha = \sim 90^\circ$ , the step velocity was considered close to zero and thus, the  $\Omega_{\text{calcite}}$  was defined as “low”; (2) when  $85^\circ < \alpha < 90^\circ$ , the step velocity was considered moderate and the  $\Omega_{\text{calcite}}$  was defined as “intermediate”; and (3) when  $\alpha < 85^\circ$ , the step velocity was considered relatively fast and the  $\Omega_{\text{calcite}}$  was defined as “high”.

**TABLE 1.** Compositions and pH for the test solutions

	pH	Mg <sup>2+</sup> :Ca <sup>2+</sup>	Ca <sup>2+</sup> :HCO <sub>3</sub> <sup>-</sup>	$\Omega_{\text{calcite}}$
		<b>Low <math>\Omega_{\text{calcite}}</math></b>		
high Mg/Ca	7.8	10	1:10	0.4
		<b>Intermediate <math>\Omega_{\text{calcite}}</math></b>		
intermediate Mg/Ca	7.9	2	1:10	0.8–1.0
		<b>High <math>\Omega_{\text{calcite}}</math></b>		
high Mg/Ca	7.9	5–10	1:10	1.1–1.2

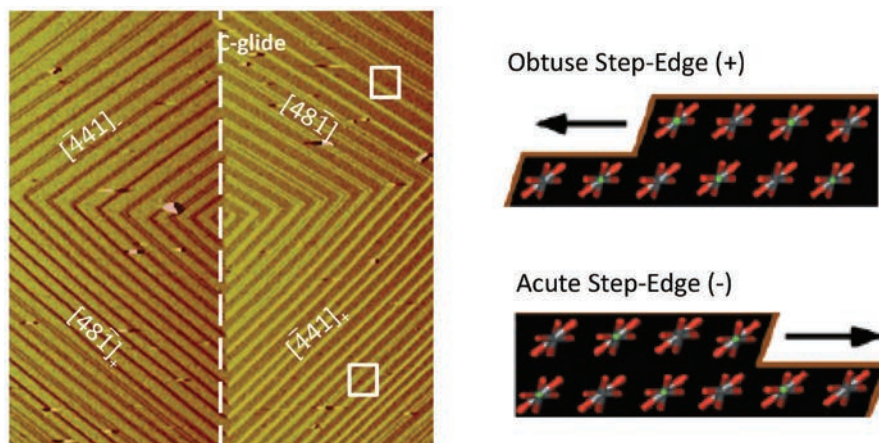


**FIGURE 1.** Anatomy of a spiral hillock ( $4 \times 4 \mu\text{m}$  view) grown at the calcite cleavage surface ( $10\bar{1}4$ ). The AFM images shown here are obtained in this study, and the molecular models are modified from Davis et al. (2004). (Color online.)

### Secondary ion mass spectrometry

Distribution of Mg at the reacted calcite surfaces was characterized using a Cameca 6f ion microprobe (secondary ion mass spectrometry) at the Department of Terrestrial Magnetism, Carnegie Institution of Washington. A focused 1 nA  $-12.5$  kV O<sup>-</sup> beam was rastered at  $50 \times 50 \mu\text{m}^2$  on the reacted calcite surface around the hillock structured area. The secondary  $\text{Mg}^+$  ions were extracted at 10 kV from the rastered area and detected using an electron multiplier at imaging mode with a spatial resolution of about 1  $\mu\text{m}$ . With the continuous rastering of the primary high energy (22.5 keV) O<sup>-</sup> ion beam for 50 or 40 s cycles, a few hundred nanometers of the sample surface were sputtered and imaged. The cycled  $\text{Mg}^+$  images confirmed that Mg was incorporated in the hillock structure rather than residual salts.

## RESULTS

The spiral hillocks formed in the absence of Mg exhibited four well-formed vicinal faces, and each of them comprises straight step edges of like orientation, identified as  $[441]$  and  $[48\bar{1}]$ , respectively. The c-glide separated the hillock into two symmetric sections of crystallographically related steps. Previous studies (Reeder and Rakovan 1999) denoted these steps as negative ( $[\bar{4}41]$  and  $[48\bar{1}]$ ) vs. positive ( $[\bar{4}41]$  and  $[48\bar{1}]$ ) based on the angle formed by these steps intersecting the  $(10\bar{1}4)$  cleavage planes. In particular, the negative steps form an acute angle of  $78^\circ$  with the  $(10\bar{1}4)$  planes, whereas the positive steps form an obtuse angle of  $102^\circ$  (Fig. 1). Upon exposure to solution  $\text{Mg}^{2+}$ , the hillock morphology was modified immediately, and developed distinct steady-state surface structures under the various solution conditions (Fig. 2).

### “Acute Syndrome” at low- $\Omega_{\text{calcite}}$ and high-Mg/Ca

The presence of  $\text{Mg}^{2+}$  at low- $\Omega_{\text{calcite}}$ , high-Mg/Ca conditions showed highly selective effects on the negative (acute) steps of the calcite hillocks. In the initial exposure to  $\text{Mg}^{2+}$ , the negative steps evened out in spacing, forming terraces of rougher texture and smaller width (Fig. 3b). As the exposure was prolonged, the negative side gradually lost the step structure and became completely amorphous in morphology (Fig. 3c). In comparison, the positive (obtuse) side was barely (or very slightly) affected by the introduction of  $\text{Mg}^{2+}$ , continuously exhibiting straight step edges along the  $[\bar{4}41]$  and  $[48\bar{1}]$  directions. Height profiles of the hillock surfaces (Fig. 3e) showed that the negative side increased in height compared to the positive side after exposure to  $\text{Mg}^{2+}$ , indicating

that the reconstruction of the negative side was not due to calcite dissolution but because of further surface growth. Compositional analyses (i.e., SIMS data) of the reacted hillock surfaces detected significant amounts of Mg to a depth of  $\sim 100$  nm in the negative side (but not in the positive side) (Fig. 3e), and thus, the combined AFM and SIMS analyses established a direct connection between the morphological change and Mg incorporation at the negative sides of the hillocks.

### Step rounding at intermediate- $\Omega_{\text{calcite}}$ and low/intermediate-Mg/Ca

The selective effect of  $\text{Mg}^{2+}$  on the hillock negative vs. positive steps became less prominent with increased solution supersaturation and decreased Mg/Ca ratios (Fig. 2c). In this scenario, the step edges exhibited varying degrees of curvature and formed a “tear-drop” shape in exposure to solution  $\text{Mg}^{2+}$ . Within the experimental duration ( $\sim 45$  min), the curved steps of the calcite hillocks advanced at relatively constant rates, and the “tear-drop” morphology of the hillocks was well maintained. It was also evident that the hillock structure was elongated in the direction parallel to the  $[42\bar{1}]$  as a result of the  $\text{Mg}^{2+}$  exposure.

### Surface segmentation at high- $\Omega_{\text{calcite}}$ and high-Mg/Ca

By comparison, the spiral hillocks underwent multiple phases of morphological changes when the solution supersaturation (i.e.,  $\Omega_{\text{calcite}}$ ) was above 1 and the Mg/Ca ratio was above 5 (Fig. 4a). In immediate exposure to  $\text{Mg}^{2+}$ , the hillock steps became curved in a similar manner as that under the intermediate- $\Omega_{\text{calcite}}$ , low/intermediate-Mg/Ca conditions (Figs. 4b and 4c). As the exposure was prolonged (after  $\sim 3$  min), linear ruptures along the  $[48\bar{1}]$  and  $[44\bar{1}]$  directions started to occur (Figs. 4d–4f). With even longer exposure, ruptures along the cleavage orientations (e.g.,  $[42\bar{1}]$ ) that connected pre-existing ones (i.e.,  $[48\bar{1}]$  and  $[44\bar{1}]$ ) were also developed (Figs. 4g–4i), segmenting the hillock surface into completely isolated plateaus with different reliefs (Appendix Supplementary Fig. 2<sup>1</sup>).

<sup>1</sup> Deposit item AM-16-55406, Supplemental Material. Deposit items are free to all readers and found on the MSA web site, via the specific issue’s Table of Contents (go to <http://www.minsocam.org/MSA/AmMin/TOC/>).

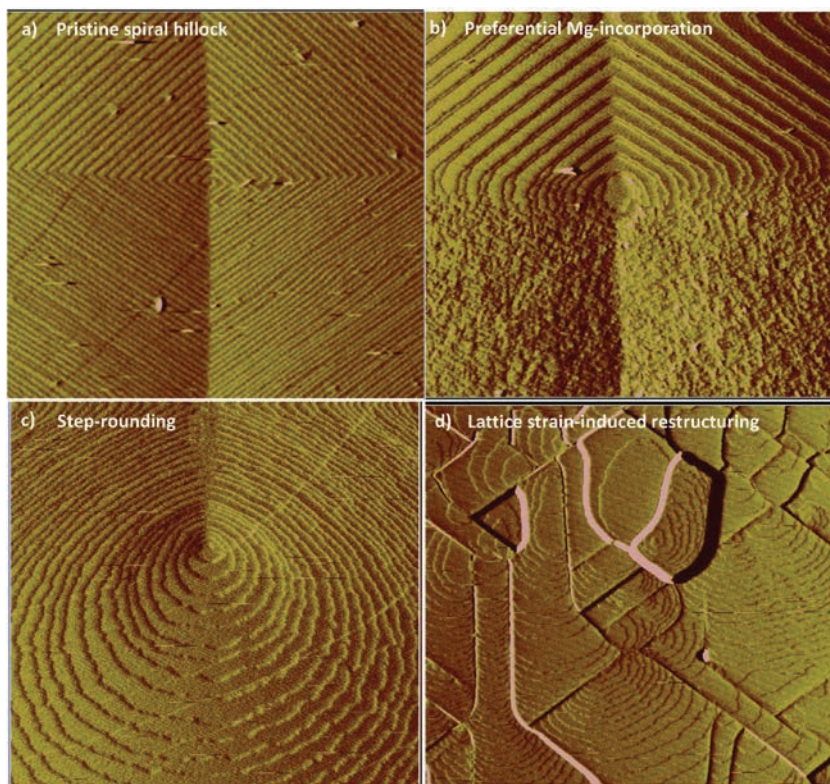


**FIGURE 2.** Morphological change of calcite spiral hillocks ( $4 \times 4 \mu\text{m}$  views) in exposure to  $Mg^{2+}$  under various growth conditions. (a) In the absence of  $Mg^{2+}$  (control); (b) at low  $\Omega_{\text{calcite}}$  and high Mg/Ca ratios; (c) at intermediate  $\Omega_{\text{calcite}}$  and intermediate Mg/Ca ratios; and (d) at high  $\Omega_{\text{calcite}}$  and high Mg/Ca ratios. (Color online.)

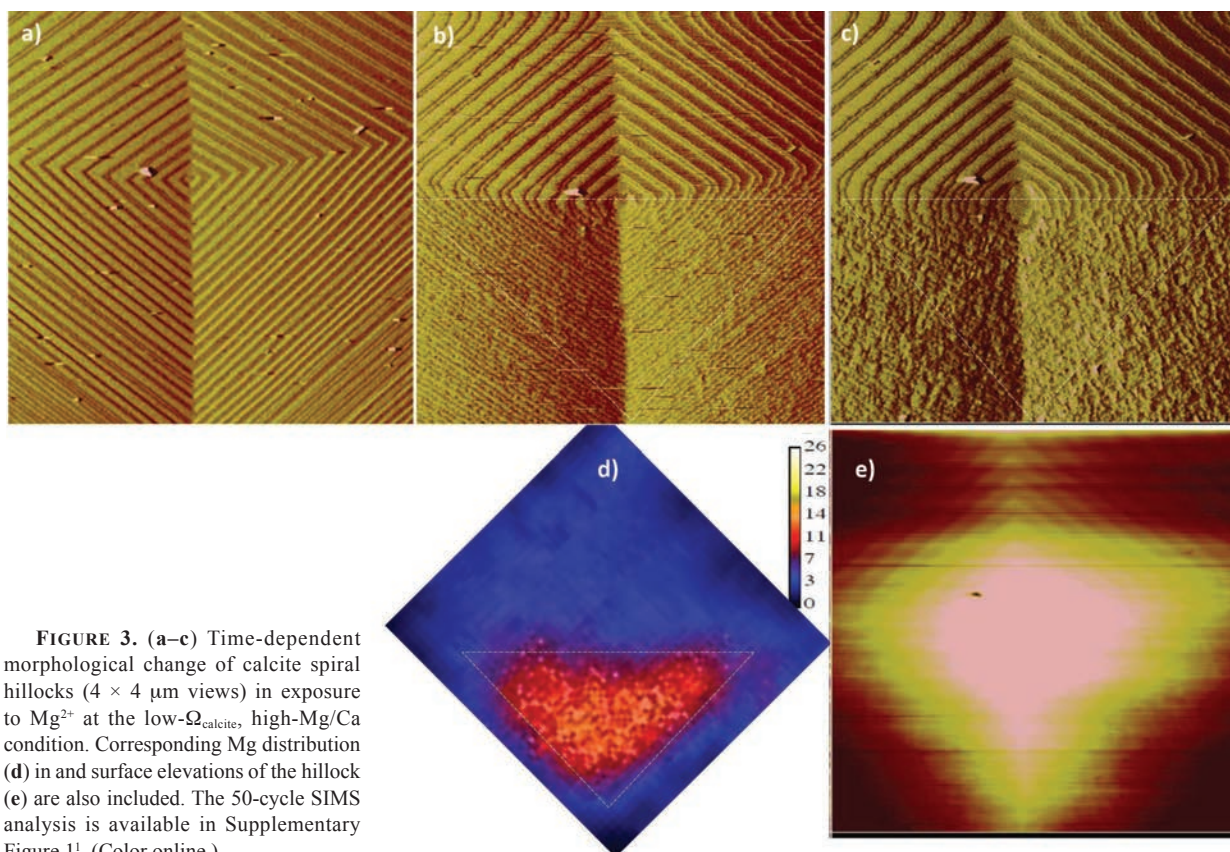


**FIGURE 3.** (a–c) Time-dependent morphological change of calcite spiral hillocks ( $4 \times 4 \mu\text{m}$  views) in exposure to  $Mg^{2+}$  at the low- $\Omega_{\text{calcite}}$ , high-Mg/Ca condition. Corresponding Mg distribution (d) in and surface elevations of the hillock (e) are also included. The 50-cycle SIMS analysis is available in Supplementary Figure 1<sup>1</sup>. (Color online.)

Several observations at the high- $\Omega_{\text{calcite}}$ , high-Mg/Ca conditions are worthy of additional notes. First, within the first  $\sim 3$  min of the experiment, only step-rounding was observed. In other words, the linear ruptures only started to occur when the steps advanced relatively far from their original locations. Second, the development of linear ruptures initiated exclusively from the periphery of the hillocks, and gradually approached the apex. Third, although the ruptures divided the original surface into separated fractions, the growth within each fraction continued via layer-spreading mechanisms. And last, the separated fractions were of different surface elevations, with the original apex still forming the highest plateau.

### DISCUSSION

Despite the proximity of Mg to Ca in the period table, the two elements differ from each other significantly when it comes to crystallization. Known distinctions between the two that are important to the present study include size (ionic radii of 114 vs. 86 pm for  $Ca^{2+}$  and  $Mg^{2+}$ ) and resultant charge density, and affinity of Mg to the acute sites and resultant stability in the corresponding steps. Taking into considerations the energetics, kinetics, and stress-strain relations in Mg-calcite growth, we will

focus below on illuminating two major relationships revealed in this study: specifically, (1) how the calcite growth rate (driven by high  $\Omega_{\text{calcite}}$ ) and solution Mg content (i.e., Mg/Ca ratios) affected the incorporation patterns and intensity of  $Mg^{2+}$  into the hillock structure; and (2) how the two factors determined the accommodation and/or release mechanisms for the structural strains resulting from the  $Mg^{2+}$  incorporation.

### $Mg^{2+}$ incorporation vs. step geometry and dynamics

Consistent with previous work (Paquette and Reeder 1990; Reeder and Rakovan 1999; Davis et al. 2000) that documented the unequal affinity of trace elements of different sizes (including  $Mg^{2+}$ ) to the crystallographically non-equivalent faces of calcite during crystal growth, our results showed that the presence of  $Mg^{2+}$  had a stronger impact toward the negative side of the calcite hillocks. In contrast to the earlier findings, however, we found this biased effect appeared to be limited only at low- $\Omega_{\text{calcite}}$  and high-Mg/Ca levels when the step velocity was low (Fig. 3) as evidenced by the SIMS result of high Mg contents in the acute side and the corresponding morphological change at these conditions. The ensuing development of the “tear-drop” and particularly the segmented surface structure at higher  $\Omega_{\text{calcite}}$

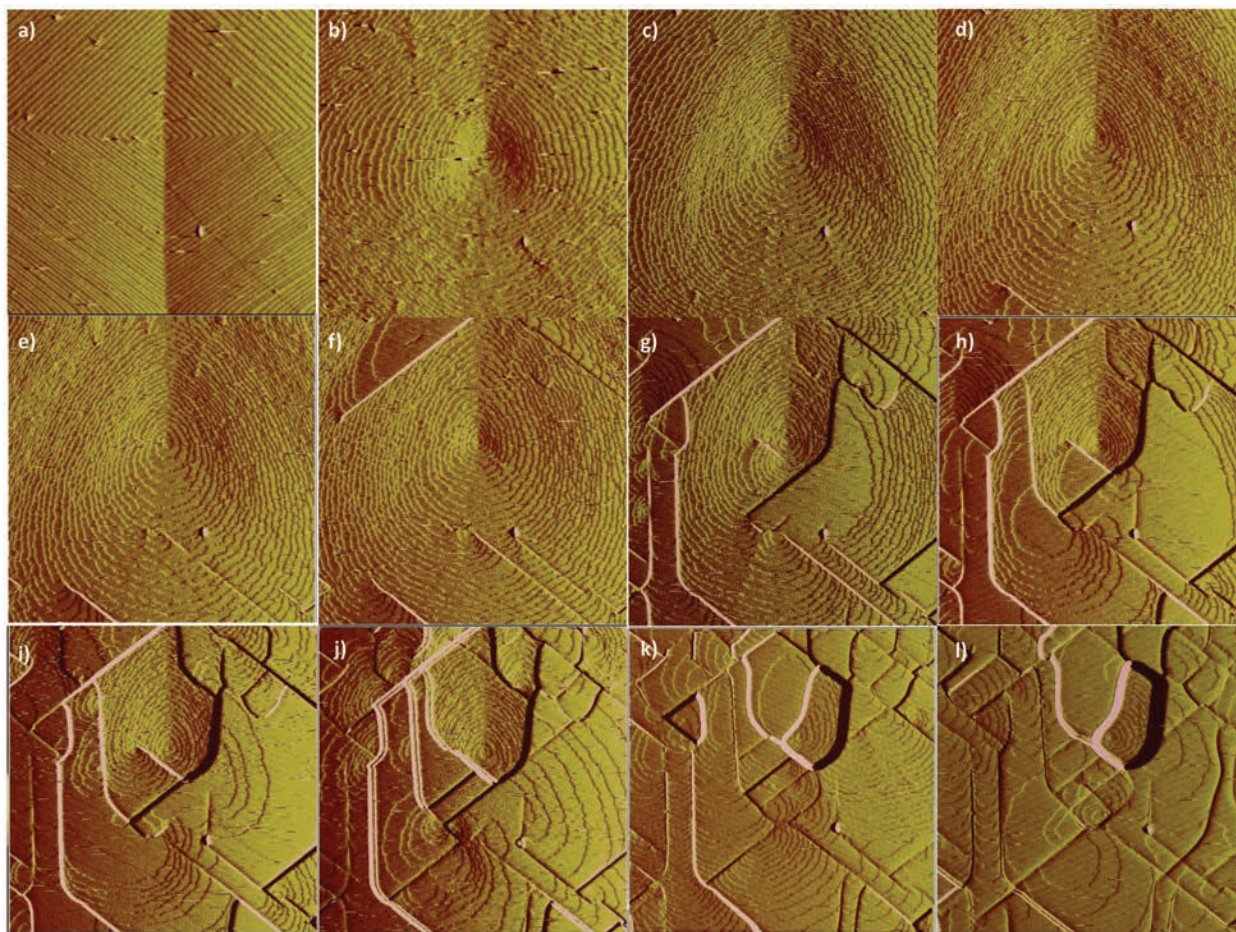


**FIGURE 4.** Time-dependent morphological change of calcite spiral hillocks ( $4 \times 4 \mu\text{m}$  views) in exposure to  $Mg^{2+}$  at high- $\Omega_{\text{calcite}}$ , high-Mg/Ca conditions. (Color online.)

and Mg/Ca levels suggests the direction-specific incorporation of Mg may not be a significant occurrence once step kinetics and solution Mg content are sufficiently high.

The asymmetric crystal structure of calcite (Fig. 1) likely represents different levels of energy barriers for the attachment of Ca<sup>2+</sup> vs. Mg<sup>2+</sup>, being a primary reason for the preferential incorporation of Mg<sup>2+</sup>. The energy compensations for Mg-CO<sub>3</sub> vs. Ca-CO<sub>3</sub> growth at different step edges of calcite from solution were previously calculated using molecular dynamic simulations (De Leeuw 2002), and the results indicated that MgCO<sub>3</sub> grows more favorably than Ca-CO<sub>3</sub> at the acute steps, and also more favorably than at the obtuse ones. It is worthy of mention that besides the preferential incorporation of Mg, our work further identifies that Mg<sup>2+</sup> incorporation can lead to loss of step structures at the negative side of the hillocks (Fig. 3). The reduced directional Mg effect at higher supersaturations, i.e., the development of the “tear-drop” morphology (Fig. 2), on the other hand, may result from a step-kinetic effect. To understand the relationship between the step velocity and the quantity of the incorporated Mg<sup>2+</sup>, we described the time-dependent adsorption of Mg<sup>2+</sup> on the step terraces of the calcite hillocks using Equation 1 below (modified from Davis et al. 2004). Specifically, the probability (P) of Mg<sup>2+</sup> capture on a terrace was expressed as a function of the lifetime of Mg<sup>2+</sup> at the terrace, determined by  $(\lambda i \cdot e^{-\Delta E_i/kT})$ , and the lifetime of the terrace itself, determined by  $(i \cdot \lambda / n \cdot v)$ , where  $\lambda$  is the total terrace width,  $n$  is the number of segments of the terrace,  $\Delta E_i$  is the adsorption energy at the  $i^{\text{th}}$  segment, and  $v$  is the hillock step velocity. In this equation, the probability (P) of Mg<sup>2+</sup> capture scales positive with terrace width ( $\lambda$ ) and is inversely correlated with the step velocity ( $v$ ). Because of the negative correlation between  $\lambda$  and supersaturation and the linear relationship between  $v$  and solute activity (the Burton-Cabrera-Frank model, Burton et al. 1951; Chernov 1961), Equation 1 inexplicitly states that increased supersaturation can result in reduced concentrations of incorporated Mg<sup>2+</sup>. This mathematical description provided theoretical explanation for the observed relationship between the step velocity and the Mg<sup>2+</sup> incorporation.

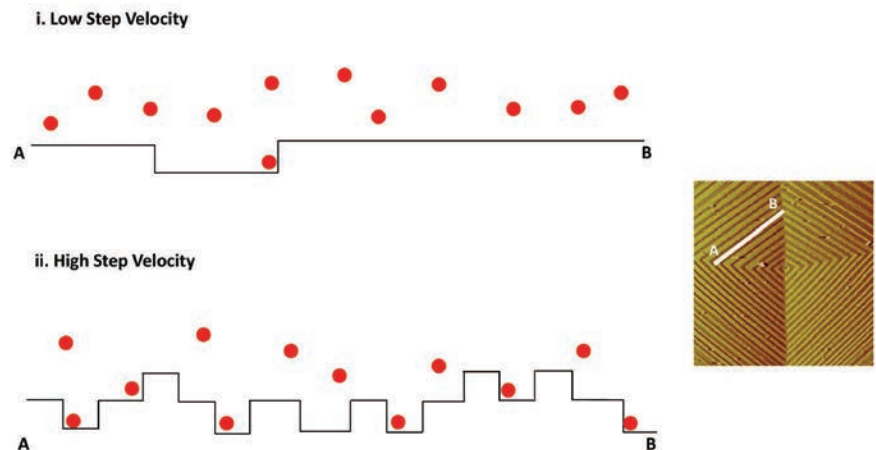
$$P = \sum_{i=0}^n \left[ \left( \frac{i \cdot \lambda}{n \cdot v} \right) \cdot \frac{\lambda}{n} \cdot e^{-\Delta E_i/kT} \right] \quad (1)$$

It is also important to note that the availability of kink sites for Mg<sup>2+</sup> adsorption and incorporation is a function of supersaturation. In the classical Burton-Cabrera-Frank model, kinks are considered to generate from thermal fluctuations at steps and, thus, are not strongly controlled by the azimuthal orientation of the steps. While this may be true at low supersaturation (i.e., small but similar kink density in both acute and obtuse sides of a growth hillock), more kinks will be present with increasing supersaturation because 1d nucleation at steps (i.e., the row-by-row growth mode) begins to contribute significantly to kink formation (Chernov et

al. 2004; Vekilov 2007; De Yoreo et al. 2009). Under low- $\Omega_{\text{calcite}}$  conditions, only limited numbers of kinks are available at acute and obtuse steps, making the probability relatively low for Mg<sup>2+</sup> to be adsorbed via sides of the kinks (Fig. 5), and therefore, the incorporation pattern of Mg is largely controlled by the energy barriers represented by step-edge geometry. By comparison, when  $\Omega_{\text{calcite}}$  is elevated and kink formation is rapid enough to create more transient sites, the adsorption of Mg<sup>2+</sup> can also occur via sides of these kinks (Fig. 5). Consequently, the step-geometry control of the Mg<sup>2+</sup> incorporation was much weakened and the growth morphology evolves from the “acute syndrome” to a “tear-drop” shape.

### Mg<sup>2+</sup>-induced strains vs. step dynamics

To a first-degree approximation, the incorporation of Mg<sup>2+</sup> into growing calcite hillocks can be considered as an epitaxial growth of newer, Mg-bearing phases onto the original Mg-free calcite (illustrated in Fig. 6). Here we point out that (1) epitaxial growth is a common mechanism to accommodate gradual compositional changes in mineral formation, and (2) deformation (e.g., stretching or compression) of the newer/older lattices is inevitable due to their different lattice parameters resultant from changing compositions. Due to the smaller ionic size of Mg relative to Ca, the newer Mg-bearing phase was stretched, whereas the older Mg-free phase was compressed (illustrated in Fig. 6b). The hillock step rounding (i.e., the “tear-drop” morphology) observed under the intermediate/high- $\Omega_{\text{calcite}}$  conditions was a direct consequence of structural stress caused by lattice mismatch between the Mg-bearing and Mg-free phases in the growing hillocks. And the variation in curvatures along the step edges suggested that different levels of structural stress were associated with different step localities (Fig. 6a). We ascribed this uneven distribution of structural stresses along the step edges mainly to the nonequivalent incorporation of Mg<sup>2+</sup> into the negative vs. positive sides of the hillocks as a combined result of the



▲ **FIGURE 5.** Schematics for the kink formation along step edges at low vs. high step velocities (top-down views). The low step velocity represents the low- $\Omega_{\text{calcite}}$ , high-Mg/Ca scenario, whereas the high step velocity represent the intermediate/high- $\Omega_{\text{calcite}}$ , intermediate/high-Mg/Ca scenarios in our study. (Color online.)

step geometry and velocity.

Contrasting to the “acute syndrome” and “tear-drop” morphology where steps lose crystallographic controls, the occurrence of segmented surface under the high- $\Omega_{\text{calcite}}$ , high-Mg/Ca conditions reflects the step’s regaining of the inherent directions and, hence, cannot be interpreted by the conventional nonequivalent Mg incorporation model. In fact, on the basis that directional Mg incorporation results in curved step formation (Fig. 3), we assume the newly developed mosaic plate boundaries in the original cleavage directions is indicative of a non-discriminative Mg incorporation at high- $\Omega_{\text{calcite}}$  at high-Mg/Ca conditions. Although the SIMS we used did not have enough resolution to resolve the composition of the macro-steps (segmental ridges) along the cleavage directions, we suspect the presence of high level Mg ions at the boundaries of the plateau, and propose that the rupture leading to the development of surface segmentation is due to the release of the  $\text{Mg}^{2+}$ -induced stress in the hillock steps. Our interpretation for this scenario is that the tensile stresses in newer phase has exceeded its elastic limit, thereby breaking the epitaxial mode of the newer and older phases via developing dislocations along energetically more favorable directions, in our case the original crystal orientations (i.e.,  $[\bar{4}81]$ ,  $[44\bar{1}]$ ) to relax the structural strains. Based on previous understanding of crystal epitaxial growth (e.g., Seifert et al. 1996; Shtukenberg et al. 2005), two components are involved in determining whether the lattice strains in the newer phase could induce the formation of dislocations: (1) the thickness ( $d$ ) of the newer phase and (2) the intensity levels of the lattice strains. In detail, the elasticity of a material layer (with homogeneous composition) decreases with its increasing thickness, and a critical value of thickness

( $d_c$ ) exists, above which the newer phase may break the epitaxy with the older phase (Stranski and Krastanow 1938). In our study, when the step velocity was high (i.e., at the high  $\Omega_{\text{calcite}}$  conditions), the thickness ( $d$ ) of the newer phase (i.e., magnesian calcite) also increased faster and thus, could reach and exceed  $d_c$  within a relatively shorter duration. This mainly explained for the development of linear ruptures within 5 min of  $\text{Mg}^{2+}$  exposure in the high- $\Omega_{\text{calcite}}$ , high-Mg/Ca scenario.

Besides the thickness of the newer phase, the intensity of  $\text{Mg}^{2+}$ -induced lattice strains also determines if dislocations can be formed at the hillock surface. Below we will discuss the effects of incorporated  $\text{Mg}^{2+}$  contents, step velocities, and step localities, respectively, on the intensity of  $\text{Mg}^{2+}$ -induced lattice strains. Higher  $\text{Mg}^{2+}$  contents in the calcite structure results in smaller lattice parameters, and therefore, with increased Mg content, higher total lattice-mismatch is generated between the newer, Mg-bearing phase and the older Mg-free phase (Fig. 6c-i vs. 6c-ii). This positive correlation between the Mg content and the lattice strains illuminated why the surface rupture only occurred at the high- $\Omega_{\text{calcite}}$ , high-Mg/Ca conditions, but not at the high- $\Omega_{\text{calcite}}$ , intermediate/low-Mg/Ca conditions within the same experimental durations ( $\sim 45$  min). In comparison, the effect of step velocities on the  $\text{Mg}^{2+}$ -induced lattice strains is less straightforward. The step velocity mainly controls the distance over which the lattice mismatch between the newer and older phases was resolved (Fig. 6c-i vs. 6c-iii). The counterintuitive point here is that this distance is likely much shortened at higher step velocity because the hillock steps transformed into the newer phase (upon exposure to  $\text{Mg}^{2+}$ ) much sooner driven by the higher growth dynamics. This understanding is corroborated

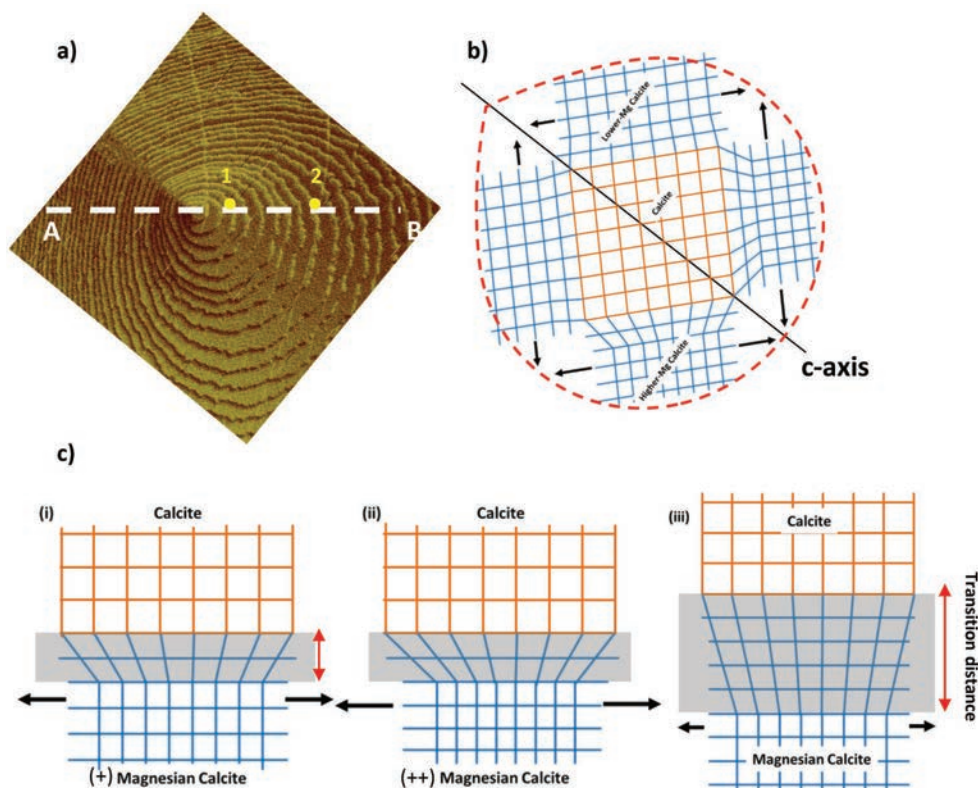


**FIGURE 6.** Major controlling factors for the hillock growth under intermediate/high- $\Omega_{\text{calcite}}$ , intermediate/high-Mg/Ca conditions. (a) A top-down image showing hillock step rounding observed in our experiments; (b) schematic illustrating the formation of tear-drop morphologies; and (c) comparison of scenarios with different strain intensities (i vs. ii) and different transition distances (i vs. iii). (Color online.)

by the observation that the surface rupture was only enabled at high  $\Omega_{\text{calcite}}$  and high step velocities in our experiments. Last, we noticed that the linear ruptures developed exclusively from the outskirts of hillocks under the high- $\Omega_{\text{calcite}}$ , high-Mg/Ca conditions. This finding indicated that the growth of different step localities were not uniform, even at the same side (e.g., Fig. 6a, locale 1 vs. locale 2). To a first-order approximation, we relate this variation in the hillock step growth to the microscopically uneven step edges resulting from the kink-formation-based growth mechanism. For example, at the locale 2 in Figure 6a, the perimeter of the steps was much longer than that at locale 1, and thus, more protrusions and depressions could be accommodated at the step edges of locale 2 without affecting the overall step velocity. This higher fluctuation associated with the microscopic step-edge structures at farther localities from the hillock apex was likely the major cause for the higher overall lattice strains and probabilities of surface rupture at these localities.

The last note about the Mg<sup>2+</sup> incorporation is that high Mg<sup>2+</sup> content could cause the calcite hillock to lose its stepped vicinal surface structure, as shown at the low- $\Omega_{\text{calcite}}$ , high-Mg/Ca conditions (Fig. 3). Both computational and experimental work found it difficult for high-Mg carbonate to crystallize at ambient *P-T* conditions due to a tighter arrangement of the Mg octahedra that restrains the CO<sub>3</sub><sup>2-</sup> groups from attaining ordered and repeatable orientations (Santillan et al. 2005; Xu et al. 2013). In our experiments at the low- $\Omega_{\text{calcite}}$ , high-Mg/Ca conditions, the observed evaporation of acute step structures may indicate that the Mg<sup>2+</sup> contents on these vicinal faces have exceeded the upper limit (~40%) allowed for the crystallization of Mg-Ca-CO<sub>3</sub>. This low- $\Omega_{\text{calcite}}$ , high-Mg/Ca scenario was likely an extreme case for the Mg<sup>2+</sup> incorporation into calcite hillocks, which occurred only at relatively static steps.

### IMPLICATION FOR BIOMINERALIZATION

The interaction mechanisms revealed for the Mg<sup>2+</sup> and growing calcite hillocks in our study may provide significant insight into carbonate biomineralization processes. For example, a multitude of previous studies on the topic showed that the distribution of Mg was spatially heterogeneous in the biogenic Mg-bearing carbonates (Stock et al. 2002, 2003; Veis et al. 2002; Vielzeuf et al. 2008; Moureaux et al. 2010). This observation, although explained by various mechanisms involving organic and/or biological molecules in the listed studies, was also evidenced under a range of  $\Omega_{\text{calcite}}$  in our experiments in the absence of organic/biological compounds, suggesting that the non-uniform distribution of Mg<sup>2+</sup> in the formed carbonate is intrinsic to the formation process of Mg-Ca-CO<sub>3</sub>. Another interesting implication of our findings for biomineralization lies in the formation mechanism of mesocrystals that were widely identified in sea urchin spines, sponge spicules, foraminifera, and calcite prisms in mussel shells, corals, or egg shells (reviewed in Oaki et al. 2006). These mesocrystals in organisms' skeletal appear polycrystalline and are usually high in Mg content, and previous studies showed that the boundaries between the sub-nanocrystals were filled with organic species or amorphous calcium carbonate (Wang et al. 1997; Oaki and Imai 2006; Sethmann et al. 2006; Killian et al. 2009; Seto et al. 2012). Controversy remains regarding the formation mechanism of calcium carbonate mesocrystals however.

Although it has been proposed that mineralization of sea urchin spicules proceeds by accumulation of nanoparticles of an amorphous calcium carbonate (ACC) precursor, which subsequently transforms into a crystal of calcite (Beniash et al. 1997; Gong et al. 2012), recent analyses of relevant mesocrystals revealed that the bulk material does not have nanoparticle and polycrystalline substructures and only a thin shell of nanoparticles is present at the crystal surface (Kim et al. 2014). Intriguingly, the observation that incorporated Mg<sup>2+</sup> can induce surface segmentation of calcite hillock structures at high- $\Omega_{\text{calcite}}$ , high-Mg/Ca conditions in our study, resonates with the fore-mentioned analyses of mesocrystals and possibly brings forward an alternative explanation for their formation mechanism.

In summary, the interactions of Mg<sup>2+</sup> with calcite hillocks were studied at various growth conditions in terms of solution  $\Omega_{\text{calcite}}$  and Mg/Ca ratios. We found that the specific combination of  $\Omega_{\text{calcite}}$  and Mg/Ca not only affected the pattern of Mg<sup>2+</sup> incorporation into calcite hillocks, but also determined if the Mg<sup>2+</sup>-induced lattice strains could be fully accommodated by the growing structure. Importantly, we revealed the interaction mechanisms between Mg<sup>2+</sup> and calcite hillocks in the various scenarios. The results of this study may provide important insight into our understanding of carbonate growth and have implication for carbonate biomineralization.

### ACKNOWLEDGMENTS

This research was financially supported by the Department of Energy Grant DE-FG02-02ER15366 to H.H.T.

### REFERENCES CITED

- Astilleros, J.M., Pina, C.M., Fernandes-Dias, L., and Putnis, A. (2000) The effect of barium on calcite {1014} surfaces during growth. *Geochimica et Cosmochimica Acta*, 64, 2965–2972.
- Beniash, E., Aizenberg, J., and Addadi, L. (1997) Amorphous calcium carbonate transforms into calcite during sea urchin larval spicule growth. *Proceedings: Biological Sciences*, 264, 461–465.
- Burton, W.K., Cabrera, N., and Frank, F.C. (1951) The growth of crystals and the equilibrium structure of their surfaces. *Philosophical Transactions A*, 243, 299–358.
- Chernov, A.A. (1961) Layer-spiral growth of crystals. *Uspekhi Fizicheskikh Nauk*, 73, 277–331.
- Chernov, A.A., De Yoreo, J., and Rashkovich, L.N. (2004) Step and kink dynamics in inorganic and protein crystallization. *MRS Bulletin*, 29, 927–934.
- Davis, K.J., Dove, P.M., and De Yoreo, J.J. (2000) The role of Mg<sup>2+</sup> as an impurity in calcite growth. *Science*, 290, 1134–1137.
- Davis, K.J., Dove, P.M., Wasylenki, L.E., and De Yoreo, J.J. (2004) Morphological consequences of differential Mg<sup>2+</sup> incorporation at structurally distinct steps on calcite. *American Mineralogist*, 89, 714–720.
- De Leeuw, N.H. (2002) Molecular dynamics simulations of the growth inhibiting effect of Fe<sup>2+</sup>, Mg<sup>2+</sup>, Cd<sup>2+</sup>, and Sr<sup>2+</sup> on calcite crystal growth. *Journal of Physical Chemistry B*, 106, 5241–5249.
- De Yoreo, J.J., Zepeda-Ruiz, L.A., Friddle, R.W., Qiu, S.R., Wasylenki, L.E., Chernov, A.A., Gilmer, G.H., and Dove, P.M. (2009) Rethinking classical crystal growth models through molecular scale insights: Consequences of kink-limited kinetics. *Crystal Growth & Design*, 9, 5135–5144.
- Elstnerova, P., Friak, M., and Fabritius, H.O. (2010) Ab initio study of thermodynamic, structural, and elastic properties of Mg-substituted crystalline calcite. *Acta Biomaterialia*, 6, 4506–4512.
- Fernandez-Diaz, L., Putnis, A., Prieto, M., and Putnis, C.V. (1996) The role of magnesium in the crystallization of calcite and aragonite in a porous medium. *Journal of Sedimentary Research*, 3, 482–491.
- Folk, R.L. (1974) The natural history of calcium carbonate: Effect of magnesium and salinity. *Journal of Sedimentary Petrology*, 44, 40–53.
- Freund, D., Rybacki, E., and Dresen, G. (2001) Effects of impurities on grain growth in synthetic calcite aggregates. *Physics and Chemistry of Minerals*, 28, 737–745.
- Given, R.K., and Wilkinson, B.H. (1985) Kinetic control of morphology, composition, and mineralogy of abiotic sedimentary carbonates. *Journal of Sedimentary Petrology*, 55, 921–926.
- Gong, Y., Killian, C.E., Olson, I.C., Appathurai, N.P., Amasino, A.L., Martin, M.C., Holt, L.J., Wilt, F.H., and Gilbert, P.U.P.A. (2012) Phase transitions in amor-

- phous calcium carbonate. *Proceedings of the National Academy of Sciences*, 109, 6088–6093.
- Hemming, N., Reeder, R., and Hart, S. (1998) Growth-step-selective incorporation of boron on the calcite surface. *Geochimica et Cosmochimica Acta*, 62, 2915–2922.
- Huang, Y., Mou, Y., Tsai, T., Wu, Y., Lee, H., Huang, S., and Chan, J. (2012) Calcium-43 NMR studies of polymorphic transition of calcite to aragonite. *Journal of Physical Chemistry B*, 116, 14295–14301.
- Killian, C., Metzler, R., Gong, Y., Olson, I., Aizenberg, J., Politi, Y., Wilt, F., Scholl, A., Young, A., Doran, A., Kunz, M., and Tamura, N. (2009) Mechanism of calcite co-orientation in the sea urchin tooth. *Journal of the American Chemical Society*, 131, 18404–18409.
- Kim, Y.Y., Schenk, A.S., Ihli, J., Kulak, A.N., Hetherington, N.B.J., Tang, C.C., Schmah, W.W., Griesshaber, E., Hyett, G., and Meldrum, F.C. (2014) A critical analysis of calcium carbonate mesocrystals. *Nature Communications*, 5, 4341.
- Lahann, R. (1978) A chemical model for calcite crystal growth and morphology control. *Journal of Sedimentary Petrology*, 48, 337–344.
- Lakhtanov, L., Bovet, N., and Stipp, S. (2011) Inhibition of calcite growth by alginate. *Geochimica et Cosmochimica Acta*, 75, 3945–3955.
- Liu, Y., Jiang, J., Gao, M., Yu, B., Mao, L., and Yu, S. (2013) Phase transformation of magnesium amorphous calcium carbonate (Mg-ACC) in a binary solution of ethanol and water. *Crystal Growth & Design*, 13, 59–65.
- Long, X., Ma, Y., and Qi, L. (2014) Biogenic and synthetic high magnesium calcite—A review. *Journal of Structural Biology*, 185, 1–14.
- Loste, E., Wilson, R., Seshadri, R., and Meldrum, F. (2003) The role of magnesium in stabilising amorphous calcium carbonate and controlling calcite morphologies. *Journal of Crystal Growth*, 254, 206–218.
- Montes-Hernandez, G., Sarret, G., Hellmann, R., Menguy, N., Testemale, D., Charlet, L., and Renard, F. (2011) Nanostructured calcite precipitated under hydrothermal conditions in the presence of organic and inorganic selenium. *Chemical Geology*, 290, 109–120.
- Moureaux, C., Perez-Huerta, A., Compere, P., Zhu, W., Leloup, T., Cusack, M., and Dubois, P. (2010) Structure, composition and mechanical relations to function in sea urchin spine. *Journal of Structural Biology*, 170, 41–49.
- Mucci, A., and Morse, J. (1983) The incorporation of  $Mg^{2+}$  and  $Sr^{2+}$  into calcite overgrowths: Influences of growth rate and solution composition. *Geochimica et Cosmochimica Acta*, 47, 217–233.
- Nishino, Y., Oaki, Y., and Imai, H. (2009) Magnesium-mediated nanocrystalline mosaics of calcite. *Crystal Growth & Design*, 9, 223–226.
- Oaki, Y., and Imai, H. (2006) Nanoengineering in echinoderms: The emergence of morphology from nanobricks. *Small*, 2, 66–70.
- Oaki, Y., Kotachi, A., Miura, T., and Imai, H. (2006) Bridged nanocrystals in biominerals and their biomimetics: Classical yet modern crystal growth on the nanoscale. *Advanced Functional Materials*, 16, 1633–1639.
- Paquette, J., and Reeder, R. (1990a) New type of compositional zoning in calcite: Insights into crystal-growth mechanisms. *Geology*, 18, 1244–1247.
- (1990b) Single-crystal X-ray structure refinements of two biogenic magnesian calcite crystals. *American Mineralogist*, 75, 1151–1158.
- (1995) Relationship between surface structure, growth mechanism, and trace element incorporation in calcite. *Geochimica et Cosmochimica Acta*, 59, 735–749.
- Parsiegla, K., and Katz, J. (1999) Calcite growth inhibition by copper (II): Effect of supersaturation. *Journal of Crystal Growth*, 200, 213–226.
- Raven, M., and Dickson, J. (1989) Fir-tree zoning—An indicator of pulsed crystallization in calcite cement crystals. *Sedimentary Geology*, 65, 249–259.
- Reddy, M., and Nancollas, G. (1976) Crystallization of calcium-carbonate. 4. Effect of magnesium, strontium and sulfate-ions. *Journal of Crystal Growth*, 35, 33–38.
- Reeder, R. (1996) Interaction of divalent cobalt, zinc, cadmium, and barium with the calcite surface during layer growth. *Geochimica et Cosmochimica Acta*, 60, 1543–1552.
- Reeder, R., and Grams, J. (1987) Sector zoning in calcite cement crystal – Implications for trace-element distributions in carbonates. *Geochimica et Cosmochimica Acta*, 51, 187–194.
- Reeder, R., and Rakovan, J. (1999) Surface structural controls on trace element incorporation during crystal growth. In J.P. Meakin, Ed., *Growth, Dissolution and Pattern-formation in Geosystems*, p. 143–162. Kluwer, Dordrecht.
- Santillan, J., Catalli, K., and Williams, Q. (2005) An infrared study of carbon-oxygen bonding in magnesite to 60 GPa. *American Mineralogist*, 90, 1669–1673.
- Seifert, W., Carlsson, N., Miller, M., Pistol, M., Samuelson, L., and Wallenberg, L. (1996) In-situ growth of quantum dot structures by the Stranski-Krastanov growth mode. *Progress in Crystal Growth and Characterization of Materials*, 33, 423–471.
- Sethmann, I., Hinrichs, R., Worheide, G., and Putnis, A. (2006) Nano-cluster composite structure of calcitic sponge spicules—A case study of basic characteristics of biominerals. *Journal of Inorganic Biochemistry*, 100, 88–96.
- Sethmann, I., Wang, J., Becker, U., and Putnis, A. (2010) Strain-induced segmentation of magnesian calcite thin films growing on a calcite substrate. *Crystal Growth & Design*, 10, 4319–4326.
- Seto, J., Ma, Y., Davis, S., Meldrum, F., Gourrier, A., Kim, Y., Schilde, U., Sztucki, M., Burghammer, M., Maltsev, S., Jager, C., and Colfen, H. (2012) Structure-property relationships of a biological mesocrystal in the adult sea urchin spine. *Proceedings of the National Academy of Sciences*, 109, 3699–3704.
- Shtukenberg, A., Astilleros, J., and Putnis, A. (2005) Nanoscale observations of the epitaxial growth of hashemite on barite (001). *Surface Science*, 590, 212–223.
- Stock, S., Barss, J., Dahl, T., Veis, A., and Almer, J. (2002) X-ray absorption microtomography (microCT) and small beam diffraction mapping of sea urchin teeth. *Journal of Structural Biology*, 139, 1–12.
- Stock, S., Ignatiev, K., Dahl, T., Veis, A., and De Carlo, F. (2003) Three-dimensional micro architecture of the plates (primary, secondary, and carinar process) in the developing tooth of *Lytechinus variegatus* revealed by synchrotron X-ray absorption microtomography (microCT). *Journal of Structural Biology*, 144, 282–300.
- Stranski, I.N., and Krastanov, L. (1938) *Abhandlungen der Mathematisch-Naturwissenschaftlichen Klasse IIb. Akademie der Wissenschaften Wien*, 146, 797–810.
- Teng, H.H., Dove, P.M., Orme, C.A., and De Yoreo, J.J. (1998) Thermodynamics of calcite growth: Baseline for understanding biomineral formation. *Science*, 282, 724–727.
- Teng, H.H., Dove, P.M., and De Yoreo, J.J. (2000) Kinetics of calcite growth: Surface processes and relationships to macroscopic rate laws. *Geochimica et Cosmochimica Acta*, 64, 2255–2266.
- Veis, A., Barss, J., Dahl, T., Rahima, M., and Stock, S. (2002) Mineral-related proteins of sea urchin teeth: *Lytechinus variegatus*. *Microscopy Research and Technique*, 59, 342–351.
- Vekilov, P.G. (2007) What determines the rate of growth of crystals from solution? *Crystal Growth & Design*, 7, 2796–2810.
- Vielzeuf, D., Garrabou, J., Baronnet, A., Grauby, O., and Marschal, C. (2008) Nano to macroscale biomineral architecture of red coral (*Corallium rubrum*). *American Mineralogist*, 93, 1799–1815.
- Wang, R.Z., Addadi, L., and Weiner, S. (1997) Design strategies of sea urchin teeth: Structure, composition and micromechanical relations to function. *Philosophical Transactions of the Royal Society of London Series B-Biological Sciences*, 352, 469–480.
- Wasylenki, L.E., Dove, P.M., and De Yoreo, J.J. (2005) Effects of temperature and transport conditions on calcite growth in the presence of  $Mg^{2+}$ : Implications for paleothermometry. *Geochimica et Cosmochimica Acta*, 69, 4227–4236.
- Xie, A., Shen, Y., Li, X., Yuan, Z., Qiu, L., Zhang, C., and Yang, Y. (2009) The role of  $Mg^{2+}$  and  $Mg^{2+}$ /amino acid in controlling polymorph and morphology of calcium carbonate crystal. *Materials Chemistry and Physics*, 101, 87–92.
- Xu, J., Yan, C., Zhang, F., Konishi, H., Xu, H., and Teng, H.H. (2013) Testing the cation-hydration effect on the crystallization of Ca-Mg-CO<sub>3</sub> systems. *Proceedings of the National Academy of Sciences*, 110, 17750–17755.

MANUSCRIPT RECEIVED MAY 5, 2015

MANUSCRIPT ACCEPTED NOVEMBER 30, 2015

MANUSCRIPT HANDLED BY LYNDIA B. WILLIAMS